Astronomy & Astrophysics manuscript no. 10235
July 30, 2008

First nonlinear force-free field extrapolations of SOLIS/VSM data

J. K. Thalmann[1], T. Wiegelmann[1] and N.-E. Raouafi[2]

[1] Max-Planck-Institut für Sonnensystemforschung, 37191 Katlenburg-Lindau, Germany
e-mail: [thalmann;wiegelmann]@mps.mpg.de
[2] National Solar Observatory, 85719 Tucson, Arizona
e-mail: raouafi@noao.edu

July 30, 2008

ABSTRACT

Aims. Our aim is to get insights in the coronal magnetic field structure in active regions and to study its temporal evolution. We are in particular interested to compare the magnetic configuration of an active region during a very quiet period with that in the course of a flare.
Methods. Within this work we use (to our knowledge for the first time) vector magnetograph data from SOLIS (Synoptic Optical Long-term Investigations of the Sun) to model the coronal magnetic field as a sequence of nonlinear force-free equilibria.
Results. We studied the active region NOAA 10960 on 2007 June 07 with three snapshots during a small C1.0 flare with a time cadence of 10 minutes and with six snapshots during a quiet period. The total magnetic energy in the active region was in the order of $3 \cdot 10^{25}$ *J*. Before the flare the free magnetic energy was about 5 % of the potential field energy. A part of this excess energy has been released during the flare and led to an almost potential configuration at the beginning of the quiet period.
Conclusions. During the investigated period the coronal magnetic energy was only a few percents higher than that of the potential field and consequently only a small C1.0 flare occurred. This has been compared with an earlier investigated active region 10540, where the magnetic energy was about 60 % higher than that of the potential field which lead to two M-class flares. The principle – free magnetic energy builds up before the flare and is released during the flare – seems to be the same for large and small flares, however.

Key words. Sun: magnetic fields – Sun: flares – Sun: corona

1. Introduction

Methods have been developed to extrapolate the observed photospheric magnetic field vector into the corona. Using the fact that the magnetic field is dominant in solar active regions (ARs) allows us to neglect non-magnetic forces, which leads to the assumption that the coronal magnetic field is force-free. Different instruments provide photospheric vector magnetograph data to be used as input for the extrapolation methods, although in the past these data had a rather low time cadence. To be able to investigate, e.g., the different evolutionary stages of solar flares in more detail, data with a high time cadence is needed – and found in form of magnetic field observations of the Sun as provided by the SOLIS Vector-SpectroMagnetograph. With a time cadence of $\approx$ 10 min the instrument is designed to measure multiple area scans of ARs which enables us for the first time to investigate the evolution of the coronal magnetic field energy with a high time cadence. Many existing studies deal with the extrapolation based on vector magnetograph data. For instance, Régnier & Priest (2007) dealt with the photospheric vector magnetic field provided by the Mees Solar Observatory Imaging Vector Magnetograph, Wiegelmann et al. (2005) used spectropolarimetric data recorded with the Tenerife Infrared Polarimeter of the German Vacuum Tower Telescope, and Thalmann & Wiegelmann (2008) performed extrapolations of Solar Flare Telescope Vector Magentograph data. However, in all these studies only one snapshot was used or, as in the latter, a sequence of vector magnetograms with a low time cadence of one magnetogram per day. Therefore, an improvement is made by applying our extrapolation technique to the high time cadence SOLIS/VSM data as described in the present study.

2. Method

2.1. Instrumentation: The SOLIS/VSM instrument

The Vector-SpectroMagnetograph (VSM; see Jones et al. 2002) on the Synoptic Optical Long-term Investigations of the Sun (SOLIS; see Keller et al. 2003) provides magnetic field observations of the Sun almost continuously since August 2003. The instrument is designed to measure the magnetic field vector everywhere on the solar disk. Full disk vector observations are done at least weekly. Multiple areas scans of ARs are also available since November 2006. In addition, longitudinal magnetic field measurements in the photosphere (at the Fe I 630.15 nm and 630.25 nm spectral lines) and chromosphere (at the Ca II 854.2 nm spectral line) are available on daily basis. Quick-look data (JPEG images and FITS files) of

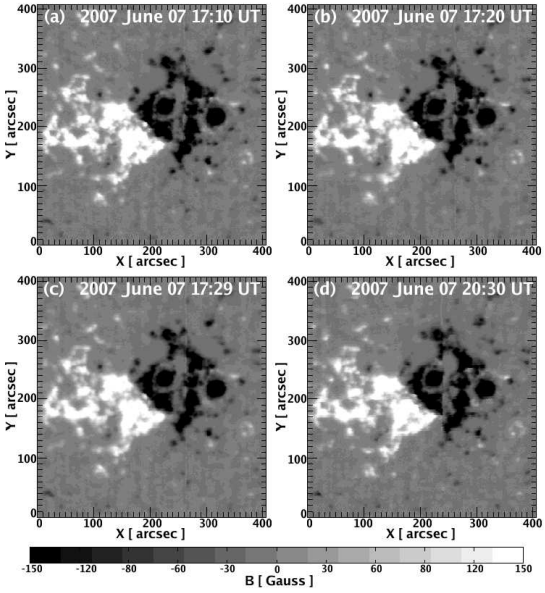

Fig. 1. Longitutional components of the SOLIS/VSM data during the C1.0 flare in panels (a) – (c) and after the flare in panel (d).

the magnetic field vector in and around automatically selected ARs (Georgoulis et al. 2008) are available on-line for the community. It provides estimates of the magnetic field strength, inclination, and azimuth (Henney et al. 2006, and references therein) which should, because of the high field strength in ARs, be quite comparable to fully inverted data only differing by a few percents. The azimuth 180°-ambiguity is solved using the Nonpotential Magnetic Field Calculation method (NPFC; see Georgoulis 2005) which does not introduce any error in the azimuth or any other quantities. Tools for full Milne-Eddington inversion are being developed to provide more accurate magnetic data especially in weak field regions.

In the time period around an C1.0 flare on 2007 June 07, three SOLIS/VSM vector magnetograms were available to use. One in the rising phase of the emission, one at the time when the flare peaked, and one in its decaying phase (at 17:10 UT, 17:20 UT, and 17:29 UT as shown in panel (a), (b), and (c) in Fig. 1, respectively). All the other magnetic field measurements on June 07 (between 20:30 UT and 21:42 UT) allow us to investigate the magnetic field structure in a period of low solar activity.

2.2. Numerics: Nonlinear force-free extrapolation

The basic equations for the computation of the nonlinear force-free magnetic field vector **B** are

$$(\nabla \times \mathbf{B}) \times \mathbf{B} = 0, \tag{1}$$

$$\nabla \cdot \mathbf{B} = 0, \tag{2}$$

where (1) expresses that the Lorentz force is forced to vanish (as a consequence of $\mathbf{j} \parallel \mathbf{B}$, where $\mathbf{j}$ is the electric current density) and (2) describes the absence of magnetic monopoles. For reviews on how to solve these equations see, e.g., Sakurai (1989), Amari et al. (1997), and Wiegelmann (2008).

A special form of force-free fields are potential magnetic fields which can be computed from the longitudinal photospheric magnetic field alone and correspond to the minimum energy state for given boundary conditions. We calculate the potential field with the help of a Fast-Fourier method (Alissandrakis 1981). In an AR only the energy exceeding that of a potential field – the so called free magnetic energy – can partly be transformed into kinetic energy during dynamic events. Therefore, nonlinear force-free (NLFF) field models are needed for a realistic estimation of the coronal magnetic field. Some of the existing methods to compute NLFF fields have been recently tested and compared by Schrijver et al. (2006), Metcalf et al. (2008), and Schrijver et al. (2008). These works revealed that the optimization method as proposed by Wheatland et al. (2000) and as implemented by Wiegelmann (2004) is a reliable and fast algorithm for this aim. This approach evolves the magnetic field to match the boundary, force-free, and divergence-free conditions by minimizing a volume integral of the form

$$L = \int_V w(x,y,z) \left(B^{-2} |(\nabla \times \mathbf{B}) \times \mathbf{B}|^2 + |\nabla \cdot \mathbf{B}|^2 \right) d^3x, \tag{3}$$

where V denotes the volume of the computational box and $w(x,y,z)$ is a weighting function (for details see Wiegelmann 2004). The SOLIS data have been preprocessed (for details see Wiegelmann et al. 2006) to bring the forced photospheric boundary closer to a force-free state in order to provide suitable boundary conditions for the minimization of (3). From the resulting potential and force-free magnetic field, one can estimate an upper limit for the free magnetic energy associated with coronal currents in the form

$$E_{free} = \frac{1}{2\mu_0} \int_V \left(B_{nlff}^2 - B_{pot}^2 \right) d^3x, \tag{4}$$

where μ_0 denotes the magnetic permeability of vacuum, and B_{pot}, B_{nlff} represent the total energy content of the potential and NLFF magnetic field, respectively. To estimate the uncertainty of the numerical result, the code has beside to the original SOLIS data also been applied to the same data with random, artificial noise in form of a normal distribution added on it ($\propto$ 1 G in the longitudinal and $\propto$ 50 G in the transversal component). The chosen noise amplitudes relate to the sensitivity of the VSM instrument. It measures the Stokes V parameter much more accurately than the parameters Q and U. While the longitudinal field is proportional to V, the transverse component is obtained through Q and U which is the source of uncertainties.

3. Results

3.1. Flare activity of NOAA AR 10960

The solar activity during the week of 2007 June 04 – 09 was dominated by NOAA AR 10960. An M8.9 flare occurred on June 04 and an M1.0 flare was fired off on June 09. Furthermore, 12 C-class flares were spread over this week and originated from this group or from the vicinity of it. The peaks in the measured solar soft X-ray (SXR) flux show only one C1.0 flare on June 07, peaking at 17:20 UT which is from interest for the present study (see Fig. 2). SOLIS data with a high time cadence are available only for June 07.

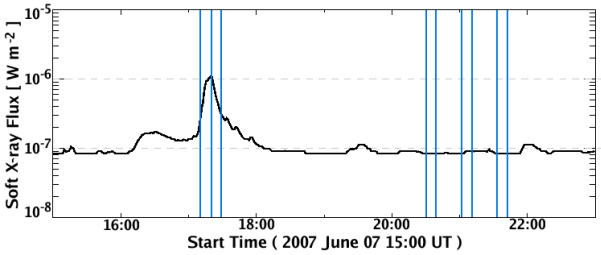

Fig. 2. Solar SXR flux on 2007 June 07 in the wavelength range of 0.1 – 0.8 nm. Vertical lines indicate when SOLIS/VSM data was available.

3.2. Global magnetic energy budget

We find for all magnetic field configurations that the energy of the extrapolated NLFF field exceeds that of the potential field (i.e., $E_{nlff} > E_{pot}$), both being in the order of 10^{25} J (see Table 1), which also holds including an estimated error of $E_{pot} \pm 0.013 \cdot 10^{25}$ J (i.e., ± 0.4 %) and $E_{nlff} \pm 0.032 \cdot 10^{25}$ J (i.e., ± 1 %). The available free magnetic energy is always in the order of 10^{24} J with an relative error of about 14 % (i.e., $E_{free} \pm 0.026 \cdot 10^{24}$ J). These uncertainty ranges have been appraised once by comparing subsequent 3D fields during the quiet period, and once by calculating the energy variation of the force-free fields after adding artificial random noise on the initial magnetograms. Both, E_{nlff} and E_{pot} were highest in the phase of increasing emission from the C1.0 flare. During the 20 min time period of the flare (17:10 UT – 17:29 UT, see Fig. 3) the magnetic energy decreased by $\Delta E_{nlff} = 2.01 \cdot 10^{24}$ J, i.e., ≈ 38 % of the available free magnetic energy became released. Although the flare was already declining at 17:29 UT it still showed a SXR-flux above background B-level (see Fig. 2). The next vector magnetogram snapshot was available only 3 hours later at 20:30 UT (see panel (d) of Fig. 1) and the free magnetic energy has decreased further, so that ≈ 88.16 % of the original amount of free energy has been released. At 20:30 UT the magnetic energy was only ≈ 0.6 % of the total energy and consequently the magnetic field is almost potential.

From Fig. 2 we see that AR10960 showed only background B-level activity (i.e., a SXR emission < 10^{-7} Wm^{-2}) already at about 18:15 UT and one might suspect that almost the entire free magnetic energy has been released up to that time. Unfortunately, no vector magnetograph data was available immediately after the declining phase of the flare so that we cannot check this supposition. For the AR studied here, the maximum excess energy of a NLFF field over the potential field was about 5 % during the investigated period. As this so called free energy is an upper limit for the available energy to drive eruptive phenomena, consequently only a small C1.0 flare was recorded. No further flares occurred between 20:30 UT and 21:42 UT for which SOLIS data was available, but five C-class flares have been recorded about 3 hours later on June 08 between 01:00 UT and 16:00 UT. However, a significant amount of free magnetic energy has built up again during the the quiet period after 20:30 UT (see Table 1 and Fig. 3) so that the energy content of the field increased and became, with some fluctuations, comparable with that at the time before the C1.0 flare.

From a visual inspection of the magnetic field lines within the extrapolation volume, we recognize some changes of the magnetic field structure in the course of the C1.0 flare (see Fig. 4). We find that the field lines show their highest vertical extent when the C1.0 flare peaked (panel (b)). Ten minutes earlier a comparable field structure is found (panel (a)), but with a lower vertical extend. Nine minutes after the flare peaked, the field line configuration finds its lowest vertical extent (panel (c)) and now more field lines of the NLFF field leave the extrapolation volume. However, at 20:30 UT, corresponding to the field configuration with the lowest energy content, the field clearly seems to be restructured, finding on average the lowest altitude. The return to an almost potential structure can be assigned to a CME as recorded by the SoHO/LASCO instrument on 2007 June 07 around 17:30 UT so that whatever magnetic helicity was bodily removed from the structure.

Table 1. Magnetic energy of the extrapolated fields.

Time [*UT*]	$E^{(1)}_{pot}$ $\left[10^{25}\ J\right]$	$E^{(2)}_{nlff}$ $\left[10^{25}\ J\right]$	$E^{(3)}_{free}$ $\left[10^{25}\ J\right]$	$E_{nlff}/E^{(4)}_{pot}$
17 : 10	3.130	3.282	0.152	1.049
17 : 20	3.122	3.272	0.149	1.048
17 : 29	2.986	3.081	0.095	1.032
20 : 30	3.024	3.042	0.018	1.006
20 : 39	3.031	3.127	0.095	1.031
21 : 02	2.969	3.084	0.116	1.039
21 : 11	2.938	3.028	0.090	1.031
21 : 33	2.939	3.125	0.185	1.063
21 : 42	2.933	3.085	0.152	1.052

[(1)]Magnetic energy of the potential and [(2)]NLFF field, [(3)]upper limit of the free energy and [(4)]nearness of the NLFF and potential field.

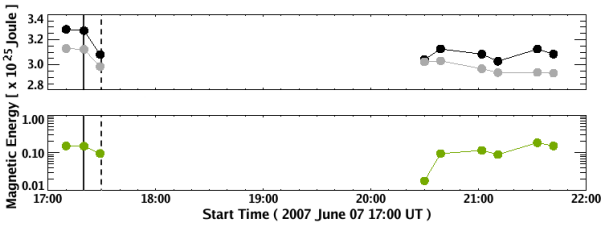

Fig. 3. *Upper panel:* magnetic energy of the potential (gray) and NLFF (black) field. *Lower panel:* upper limit for the free magnetic energy (shown on logarithmic scale). Solid and dashed lines represent the recorded C1.0 flare and CME, respectively.

4. Discussion

We investigated the coronal magnetic field associated with the NOAA AR 10960 on 2007 June 07 with the help of SOLIS/VSM data. Three vector magnetograms with a time cadence of ≈ 10 min were available to investigate the magnetic energy content of the coronal field in the course of an C1.0 flare and six further snapshots have been taken to analyze a very quiet time about three hours after the flare. Before as well as after the small flare, the magnetic field energy was

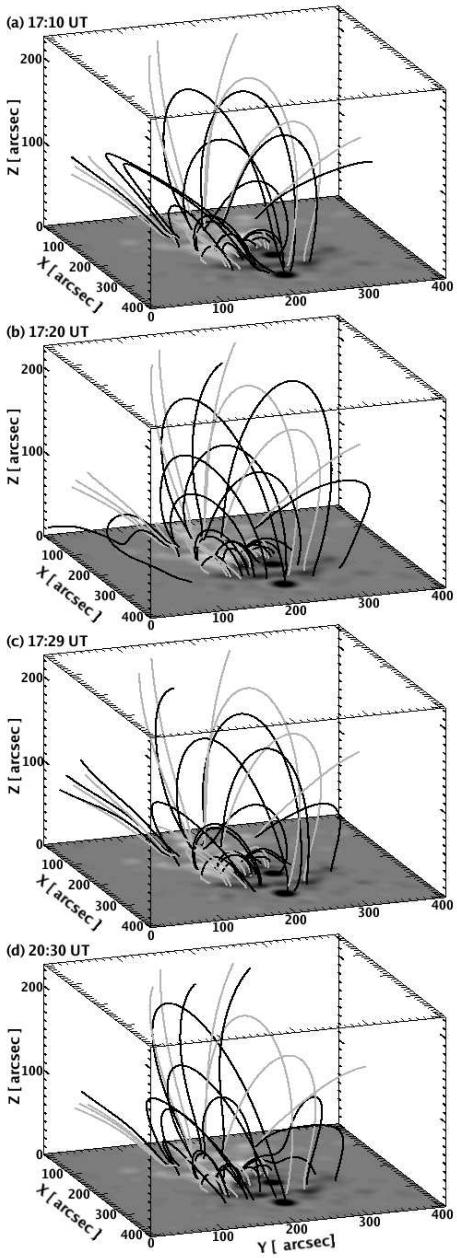

Fig. 4. Panels (a), (b), and (c) show the magnetic field configuration during the C1.0 flare. Panel (d) shows the minimum energy configuration. Shown are field lines of the potential (gray) and NLFF (black) field. For better visibility the *z*-axis is drawn elongated.

$E_{nlff} \approx 3 \cdot 10^{25}$ J. The NLFF field energy exceeded that of the corresponding potential field by about 5 % and had a free energy $E_{free} \approx 1.5 \cdot 10^{24}$ J before the flare. As a consequence of the flare/CME this free magnetic energy reduced almost by a factor of 10 and led to an almost potential configuration. Six snapshots taken within about 70 min during a very quiet period of 3 – 4 hours after the flare showed again an increase of free magnetic energy. According to the fact that the estimated free magnetic energy was always only about 5 % of the total energy, no large eruption was produced by AR 10960.

This is clearly different from the flaring AR 10540 as observed in January 2004 which has been analyzed in a previous work with the help of vector magnetograph data from the Solar Flare Telescope in Japan with a time cadence of about 1 day. In this AR the free energy was $E_{free} \approx 66$ %, high enough to power an M6.1 flare (for details see Thalmann & Wiegelmann 2008). The activity of that earlier investigated AR 10540 was significantly higher compared with the data analyzed in the current paper and so was the total magnetic energy. However, despite these differences we found also common features. Magnetic energy builds up before the flare and a significant part of the excess energy becomes released during the flare. The high amount of free magnetic energy available in AR 10540 led to M-class flares, while the relative small amount of free energy in AR 10960 powered only a small C-class flare. In both cases all three components of the vector magnetogram changed during the flare, but the energy decrease of the NLFF field was always higher than that of the potential field, i.e., the energy release is more related to the change of the transverse magnetic field components – which correspond to field aligned electric currents in the corona – than to that of the longitudinal one.

Acknowledgements. SOLIS/VSM vector magnetograms are produced cooperatively by NSF/NSO and NASA/LWS. The National Solar Observatory (NSO) is operated by the Association of Universities for Research in Astronomy, Inc., under cooperative agreement with the National Science Foundation. J. T. is supported by DFG-grant WI 3211/1-1, T. W. by DLR-grant 50 OC 0501, and N.-E. R. by NSO and NASA grant NNH05AA12I. We thank B. Inhester for helpful discussions.

References

Alissandrakis, C. E. 1981, A&A, 100, 197
Amari, T., Aly, J. J., Luciani, J. F., Boulmezaoud, T. Z., & Mikic, Z. 1997, Sol. Phys., 174, 129
Georgoulis, M. K. 2005, ApJ, 629, L69
Georgoulis, M. K., Raouafi, N.-E., & Henney, C. J. 2008, in ASP Conf. Ser., ed. R. Howe, R. W. Komm, K. S. Balasubramaniam, & G. J. D. Petrie, Vol. 383, 107
Henney, C. J., Keller, C. U., & Harvey, J. W. 2006, in ASP Conf. Ser., ed. R. Casini & B. W. Lites, Vol. 358, 92
Jones, H. P., Harvey, J. W., Henney, C. J., Hill, F., & Keller, C. U. 2002, in ESA SP, Vol. 505, Magnetic Coupling of the Solar Atmosphere, ed. H. Sawaya-Lacoste, 15
Keller, C. U., Harvey, J. W., & Giampapa, M. S. 2003, in Innovative Telescopes and Instrumentation for Solar Astrophysics., ed. S. L. Keil & S. V. Avakyan, Vol. 4853, 194
Metcalf, T. R., Derosa, M. L., Schrijver, C. J., et al. 2008, Sol. Phys., 247, 269
Régnier, S. & Priest, E. R. 2007, ApJ, 669, L53
Sakurai, T. 1989, Space Science Reviews, 51, 11
Schrijver, C. J., DeRosa, M. L., Metcalf, T., et al. 2008, ApJ, 675, 1637
Schrijver, C. J., Derosa, M. L., Metcalf, T. R., et al. 2006, Sol. Phys., 235, 161
Thalmann, J. K. & Wiegelmann, T. 2008, A&A, 484, 495
Wheatland, M. S., Sturrock, P. A., & Roumeliotis, G. 2000, ApJ, 540, 1150
Wiegelmann, T. 2004, Sol. Phys., 219, 87
Wiegelmann, T. 2008, JGR (Space Physics), 113, 3
Wiegelmann, T., Inhester, B., & Sakurai, T. 2006, Sol. Phys., 233, 215
Wiegelmann, T., Lagg, A., Solanki, S. K., Inhester, B., & Woch, J. 2005, A&A, 433, 701